

Mechanical and Tribological Properties of Alumina Toughened Zirconia Composites through Conventional Sintering and Microwave Sintering

K. L. Meena¹ · Ch. Suresh Vidyasagar² · D. Benny Karunakar¹

Received: 22 December 2019 / Accepted: 14 May 2020 / Published online: 5 June 2020
© The Indian Institute of Metals - IIM 2020

Abstract The present study investigates the relative density, mechanical and tribological properties of 3 mol% yttria-stabilized zirconia composites reinforced with 10 vol% of alumina through both conventional sintering and microwave sintering (CS and MW). The variations in mechanical and tribological properties were correlated to the corresponding microstructures. Wear tests were carried out on the composite samples against EN30 grade stainless steel disk with 320-grade emery paper for a sliding distance of 1500 m under dry sliding condition. Wear rate and coefficient of friction of the developed composite were evaluated with varying normal loads in the range of 20–200 N with corresponding sliding velocities of 0.79 m/s, 1.4 m/s, 1.8 m/s and 2.4 m/s, respectively. The maximum value of wear rate and COF of the MW samples were 51.21% and 24.59%, respectively, which were lower compared to that of CS.

Keywords Alumina toughened zirconia (ATZ) · Conventional sintering (CS) · Microwave sintering (MW) · Sliding velocity · Coefficient of friction (COF) · Wear rate

1 Introduction

Zirconia toughened alumina (ZTA) composites are known as a class of new-generation ceramics with a fracture toughness that is four times higher than that of alumina alone [1]. Going back in time, zirconia was introduced to alumina as an aid to densify alumina, and it is only later that zirconia was used as a reinforcement particulate to alumina for improving the toughness [2, 3]. Several studies have been conducted in the recent past on the use of ZTA to improve mechanical properties. Examples include ZTA used as reinforcement in the composites comprising of different matrices such as Fe [4], Al [5], chromium cast iron [6], niobium (Nb) [7]. Also, on the other hand, some studies have been conducted using ZTA as reinforcement for wear applications, which include the findings of Qui et al. [8] who reinforced ZTA to Fe matrix and reported a significant improvement in the wear properties of the composite as compared to the matrix material. Perrichon et al. [9] used ZTA as the matrix to develop ceramic composites for the orthopedic hip joint. After conducting nano-strip wear tests, they concluded that these ZTA hip joints could provide long-term resistance against hydrothermal aging.

In the previous decade, many studies have been focused on developing alumina toughened zirconia (ATZ) ceramic composites with improved mechanical properties. Examples include, Zhang et al. [10] investigated the influence of (0.25, 2 and 2.5 wt%) alumina content on the temperature degradation of (2, 2.5 and 3 mol%) yttria-stabilized TZP for dental applications. Rittidech et al. [11] discussed the effect of adding 1–8 wt% Y_2O_3 on phase formation and fracture toughness of developed $Al_2O_3-xZrO_2-Y_2O_3$ (AZY) ceramics. The addition of Y_2O_3 contents did not influence the grain shape of AZY ceramics. Basha et al.

✉ D. Benny Karunakar
benny.karunakar@me.iitr.ac.in

¹ Department of Mechanical and Industrial Engineering, Indian Institute of Technology Roorkee, Roorkee, Uttarakhand 247667, India

² Department of Metallurgical and Materials Engineering, Indian Institute of Technology Roorkee, Roorkee, Uttarakhand 247667, India

[12] developed ZrO_2 composites reinforced with SrO-doped Al_2O_3 and reported that reaction sintering leads to dense composite ceramics with finer matrix grains with nearly homogeneous multiphase microstructures. Bansal [13] developed dense and crack-free 10-mol% yttria-stabilized zirconia (10 YSZ)-alumina composites, containing 0–30 mol% of alumina through hot pressing and achieved lighter, stronger, and stiffer composites.

Wear is defined as the process of material removal from the surface of one component due to the interaction between mating and when rubbed against another surface. Due to several numbers of contact surfaces and moving parts involved in machines, the parts lose their reliability. They tend to fail before their life time due to wear and therefore, wear behavior is an essential factor to be considered by the manufacturers in the development of high-quality durable wear-resistant materials for new and advanced machines [14]. It is worthwhile to mention that wear is not a material property but a consequence of material usage and it varies from material to material based on the conditions [15]. However, tribo-chemical reactions between two surfaces occur dynamically when both mechanical and thermal effects are acting simultaneously during the operating conditions. However, there are several diverse effects on the wear fracture mechanism, such as abrasion, adhesion, and fatigue, and each result has its specific mechanisms. Hamilton [16] studied the stress field created by a circular sliding contact. They reported that the stress beneath a circular region of contact subjected to a normal and tangential force is distributed hemispherically over the sliding surface. They also pointed out that for ceramic materials, the value of tensile stress is more important than the yield parameter as one of the principal stresses is tensile near the edge of the contact surface. This tensile stress acts in a radial direction leading to a ring crack even at a low COF value.

These interesting and excellent tribological properties and other mechanical properties at high temperatures make them more useful in applications such as ballistic armor [17], cutting tool inserts [18], biomedical [19], and within no time the applications of these ZTA composites will extend into industries such as aerospace, power generation, automobile. The ceramic-based materials such as nitride and carbide (e.g., SiC, Si_3N_4) have excellent hardness, and silicon nitride is used for a ball bearing. However, the problem with these materials is that, they have issues related to oxidation and corrosion. On the other hand, materials such as Al_2O_3 and ZrO_2 do not suffer from oxidation, and the nature of these materials is brittle. Though the hardness of alumina and zirconia is lower than that of carbide and nitride, their low cost makes them very attractive and go-to materials for the manufacturers. Moreover, the toughness and wear properties of alumina

can be enhanced by adding zirconia. However, the properties of ZTA must be improved by reinforcing the material. It has been reported in the literature that the addition of up to 1 wt% of MgO to ZTA-TiO₂ composite can significantly improve all the mechanical properties along with wear [20, 21]. Also, the addition of carbon nanotubes up to 0.1 wt% to ZTA can suppress grain growth in the ZTA matrix and hence improve the mechanical properties [22]. Azhar et al. [23] discussed the microstructure, mechanical properties and wear performance of ceramic cutting inserts produced from Al_2O_3 , yttria-stabilized zirconia and magnesium oxide system. The increase in hardness of the cutting insert is mainly contributed by small-sized Al_2O_3 grains. De Couto et al. [24] reported that the addition of CNT in the ceramic and composite caused a general increase in densification, hardness, flexural strength and fracture toughness of ZTA composites and the addition of 0.1 wt% of CNT yielded the best results.

From the literature, it can be found that most of the studies were conducted at a micro-scale with a conventional sintering method and very few studies were found to have focused at the nanoscale. Recently, microwave sintering (MW) process came into the picture as a novel sintering technique compared to conventional sintering (CS), especially for materials that require high-temperature sintering [25]. Moreover, MW also overcomes the drawbacks such as poor and incomplete sintering [26], prolonged sintering times, low heating rates [27], that are encountered in CS.

Therefore, the main objective of the present study is to develop and evaluate the mechanical, metallurgical and tribological properties of ZrO_2 matrix composites reinforced with Al_2O_3 by using both CS and MW processes separately. Also, the average grain size, relative density, microhardness, fracture toughness, wear rate and COF of the composite samples developed through CS and MW have been compared.

2 Experimental Methods

2.1 Materials

In this present work, nanopowder of 3 mol% yttria-stabilized zirconia (3-YSZ) (99% purity, 5.68 g/cm³ theoretical density and 30 nm primary size of monoclinic particles) was used as matrix material. The reinforcement used in the present study was commercially available α - Al_2O_3 nanopowder (99% purity, 3.95 g/cm³ theoretical density and 100 nm mean particle size). This high purity, thermally reactive type powders were procured from “Nano Partech” Chandigarh, India. Both the powders were used as starting materials.

2.2 Development of the Composites

The steps involved in the preparation of ceramic-based nanocomposites consisted of reinforcing Al_2O_3 to the zirconia matrix and sintering them separately using CS and MW processes. Two different hybrid composite samples with the intended compositions shown in Table 1 were sintered by conventional sintering and microwave sintering.

For clarity of the composites developed, a flow chart with as-received materials with stepwise experimentation procedure is shown in Fig. 1.

The powders were weighed according to the proportions shown in Fig. 1 and hand-blended using an agate mortar and pestle with polyvinyl alcohol (PVA) as a binder. Each powder sample was blended manually for 40 min. After blending, the powders were dried at 50 °C to remove the moisture content, and then the powders were sieved to remove the agglomerated particles and other impurities. Polyvinyl alcohol was used as a binder to avoid cracking during compaction and sintering process as the green strength of these composites was inferior and could break while handling. A muffle furnace was used to sinter the compacted green composite samples with 10 vol% of Al_2O_3 reinforced to 3 mol% YSZ matrix, while a microwave furnace was used to sinter the same compositions as the first set. The MW furnace (customized furnace, Omicron Scientific Equipment Company, Dwarka, New Delhi, India) was used to sinter the samples in a vacuum with a power supply of 1.5 kW. The infrared radiation thermometer was used to control the sintering temperature of the sintered samples. It was focused and concentrated on the surface of the test sample through a small circular aperture in the wall of the test cell. The green samples were sintered using the susceptor material of SiC within the microwave furnace at 2.45 GHz, which acted as a hybrid heating source. The sintering process began at room temperature and was continued for a constant period until the end sintering was achieved, which was then followed by cooling. The range of process parameters used in the present CS and MW is given in Table 2.

2.3 Characterization Methods

For the microstructure evaluation, samples were given better polishing, and then thermal etching was applied. In

the thermal etching method, the samples were heated up to 1000 °C or below their melting point temperature and then cooled down up to 250 °C, after that applied chemical etching (H_3PO_4 acid) for 2 min [28]. The actual density of sintered samples was measured using standard Archimedes' principle, and the theoretical density was measured using the rule of mixtures. FE-SEM was used to analyze the microstructure. The average grain size of the sintered samples was determined using a linear intercept approach with the help of the "Image J" analysis software program. The microhardness value was measured using a computerized Vickers hardness testing machine with a load of 300 grams for a dwell time of 10 Sec. In the present experimentation, the value of c/a ratio obtained was higher than 2.5. Therefore, the composites belonged to the radial-median crack system, as reported in our recent papers [22, 24]. Thus, the Anstis equation is favorable to apply for calculating the fracture toughness of the developed composite samples. For each sample, for accuracy and precision, ten indents were taken at different places of the sample by using a macro-Vickers indenter machine. The fracture toughness (K_{IC}) was calculated using the Anstis relation as shown in (Eq. 1) [29].

$$K_{\text{IC}} = 0.016 \left(\frac{E}{H_V} \right)^{\frac{1}{2}} \frac{P}{c^{\frac{3}{2}}} \quad (1)$$

where p —indenter load, c —radial crack length, E —overall Young's modulus, which is calculated using the mixture rule, a —half of the indentation diagonal, and H_V —Vickers hardness.

2.4 Tribological Studies

The developed composite samples were subjected to wear test using a pin-on-disk apparatus. Table 3 gives various parameters and their corresponding values that were used in the characterization of COF and wear rate. The selection of parameters like normal load, sliding velocity, and duration of rubbing chosen for conducting wear test on the developed composites were the minimum values where the actual wear of the sample started to occur. Below these values, wear did not occur. Normally, COF values varied for a certain duration of rubbing and after that, it remained constant in the entire experiment [30]. Therefore, in the present study, the period of rubbing was kept constant in

Table 1 Intended compositions for tribological studies of ATZ composite

Developed composite	Al_2O_3 (vol%)	ZrO_2 (vol%)	Sintering temperature (°C)
ATZ through CS	10	90	1600
ATZ through MW	10	90	1600

Fig. 1 Flow diagram of the present work showing stepwise experimentation procedure

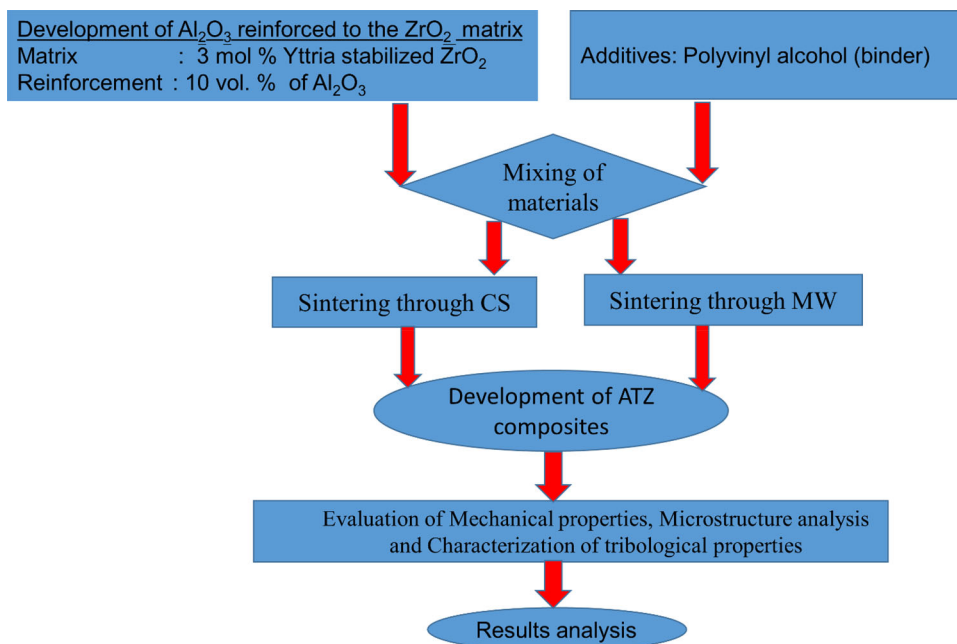


Table 2 Various process parameters and their ranges of CS and MW

Parameter	CS process	MW process
Pressure	200 MPa (hydraulic pressure)	200 MPa (hydraulic pressure)
Sintering temperature	1600 °C	1600 °C
Heating rate	5 °C/min	25 °C/min
Holding time	6 h	1 h
Sintering environment	Vacuum (10^{-6} torr)	Vacuum (10^{-6} torr)

Table 3 Various parameters were used in tribological studies

S. no.	Parameters	Operating conditions
1	Normal load	20–200 N
2	Sliding velocity	0.79 m/s, 1.4 m/s, 1.8 m/s and 2.4 m/s
3	Disk material	EN30 steel, 62 HRC (standard hardness)
4	Pin materials	Developed ceramic composite samples
5	Surface condition	Dry
6	Duration of rubbing	10 min
7	Sliding distance	1500 m

the entire experiment. Other parameters were calculated accordingly.

The pin-on-disk apparatus pointing out various parts are shown in Fig. 2.

The pin-on-disk apparatus comprised of pin (the sample) with the spherical surface at the tip, and a circular rotating disk was placed in a perpendicular direction to the spherical surface pin. The dimensions of the pin were as follows,

15 mm diameter and 30 mm long. The circular track on which the samples slide had 100 mm diameter, with a sliding duration of 10 min for a sliding distance of 1500 m. The pin was held with a jaw in the apparatus, and the motion of rotation provided to the disk resulted in wear of pin on a fixed path on the disk. All the experiments were performed using 320-grade emery paper placed on the surface of an EN30 flat steel disk. The load on the spherical

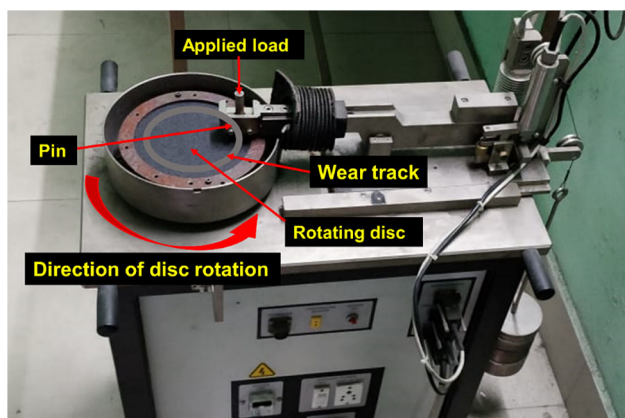


Fig. 2 Pin-on-disk apparatus used in the present study

pin was applied by placing weights on the arm attachment of the apparatus. A computer was attached to the apparatus to provide results and graphs which were connected to a data acquisition system. The COF and wear rate was calculated using Eqs. 2 and 3, respectively [31].

$$\text{Specific wear rate } (W_s) = (\nabla V / FXL) \quad (2)$$

$$\text{Coefficient of friction } (\mu) = (f / N) \quad (3)$$

where (∇V) = Wear volume loss, N = Applied normal load, L = Sliding distance, μ = Coefficient of friction, f = Friction force.

3 Results and Discussion

3.1 XRD Analysis

Figure 3a shows the XRD pattern of the as-received 3 mol% yttria-stabilized zirconia (3YSZ) powder. From Fig. 3a, it could be observed that zirconia was present in two phases namely tetragonal phase (designated as t, ICDD file No. 072-7115) and monoclinic phase (designated as m, ICDD file No. 037-1484). The tetragonal zirconia (t-ZrO₂) phase exhibited the highest peak intensity while the monoclinic zirconia (m-ZrO₂) phase exhibited few minor peaks.

The XRD analysis was carried out for phase analysis of the ATZ sintered samples, which were prepared through CS and MW sintering and the XRD peaks are shown in Fig. 3b. Various phases of tetragonal zirconia (t-ZrO₂) (designated as t, ICDD files No. 01-083-0113) and alumina (α -Al₂O₃) (designated as α , ICDD files No. 00-010-0173) and a few amount of monoclinic zirconia (m-ZrO₂) (designated as m, ICDD files No. 01-078-1807) were observed in the XRD pattern. The tetragonal phase of ZrO₂ was seen as a stable phase. All the peaks of phase analysis through

CS-sintered and MW-sintered samples were found to be almost the same, and there were no secondary phases. The highest peak intensity of tetragonal t-ZrO₂ was detected at an angle of 30°. The m-ZrO₂ phase got fully transformed into t-ZrO₂, with the presence of 3 mol% yttria-stabilized zirconia. It was observed that the MW-sintered sample exhibited a lesser amount of monoclinic phase of ZrO₂. In the present study, despite the same parameters, different heating and cooling rates were applied to the composites by CS and MW during sintering due to their operating mechanisms. During MW sintering, due to its fast heating and cooling rates, the large fraction of finer t-ZrO₂ crystallites than the larger m-ZrO₂ phases were retained, which led to better microstructure as well as improved densification of the material. On the other hand, during CS, high ratios of m-ZrO₂ were retained due to the long periods of heating and cooling that poorly improved the microstructure.

3.2 Microstructure Analysis

The microstructure evaluation of the developed ATZ composites was carried out using a field emission scanning electron microscope (FE-SEM) and backscattered electron (BSE) detectors. These composites were developed with Al₂O₃ reinforced to the ZrO₂ matrix through CS and MW, respectively, are shown in Fig. 4. The alumina grains (dark gray grains) were distributed homogeneously in the zirconia (small white grains) matrix. Compared to CS samples, MW samples exhibited smaller alumina grains that were homogeneously distributed in the zirconia matrix, as seen in Fig. 4d.

Since the developed composite samples were non-conductive, they were coated with a thin gold layer to make them conductive before the FE-SEM examination. Figure 4a–d shows the FE-SEM micrographs of CS and MW-sintered composites, respectively, with different magnification and mode. From Fig. 4a, b, it could be observed that the white and dark gray phases were t-ZrO₂ and Al₂O₃, respectively (as pointed out with arrows). Moreover, uniform distribution of the reinforced particles and close packing of the matrix grain was observed, which led to high-density composites. From Fig. 4a, c it could be observed that even though the uniform distribution of the reinforced particles was achieved, grain size was not as significant as that was found in the MW composite samples despite being provided with the same sintering temperature. However, from Fig. 4a–d, it could be noticed that all the samples attained full density and homogeneously dispersed grains of Al₂O₃ and ZrO₂ in the alumina matrix.

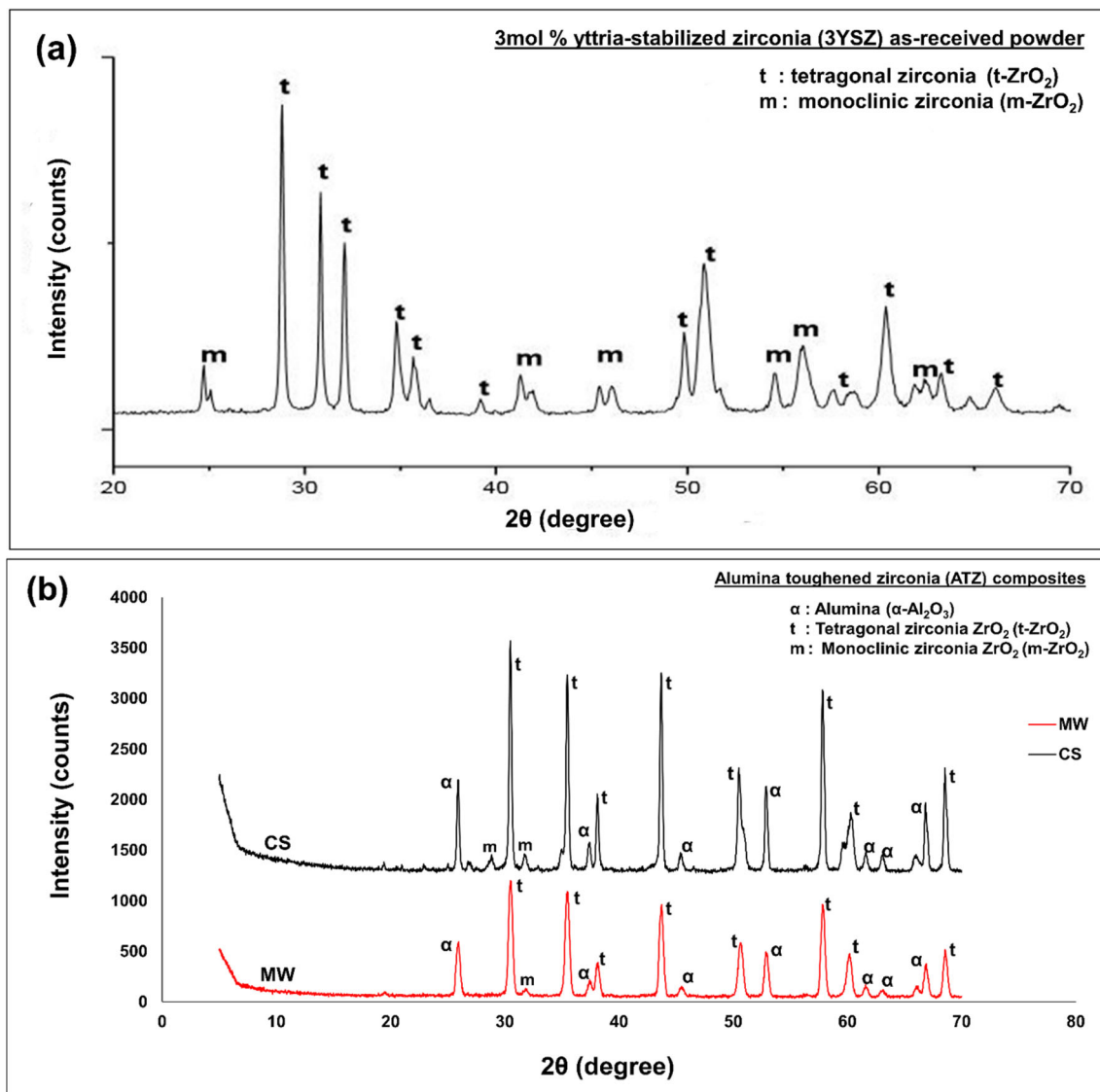


Fig. 3 X-ray diffraction patterns showing **a** peak intensities of as-received 3 mol% yttria-stabilized zirconia powder, **b** ATZ composites developed through CS and MW

3.3 EDS Analysis

Energy-dispersive X-ray spectroscopy (EDS) of the developed ATZ composite samples reinforced with 10 vol% of Al₂O₃ to the ZrO₂ matrix is shown in Fig. 5.

According to the EDS of the ATZ sintered samples, which are shown in Fig. 5, the addition of 10 vol% of Al₂O₃ reinforced to the ZrO₂ matrix was observed to exhibit a minimum value of Al element of 3.87 wt% and the maximum value of Zr element of 69.72 wt% in the composite samples sintered through CS as demonstrated in Fig. 5c. In comparison, the maximum value of Al element of 6.14 wt% and the minimum value of Zr element of 50.77 wt% were obtained in the MW-sintered composite samples as demonstrated in Fig. 5d. Generally, we know that

alumina is a hard material and zirconia is a tough material. The hardness of alumina is more than that of zirconia. Therefore, the higher value of the Al₂O₃ element found in the composites indicated an improvement in the hardness. In comparison, the higher value of the ZrO₂ element indicated an improvement in the fracture toughness. This could be attributed to the stress-induced martensitic transformation of stable t-ZrO₂ to m-ZrO₂ in the stress field around a propagating crack that enhanced the toughness of zirconia ceramics as seen from Fig. 3. The MW-sintered sample exhibited higher values of wt% of Al and from the results, it was observed that they showed better tribological behavior compared to CS composite samples. The properties of five samples with the same composition and developed ATZ composites were investigated like relative

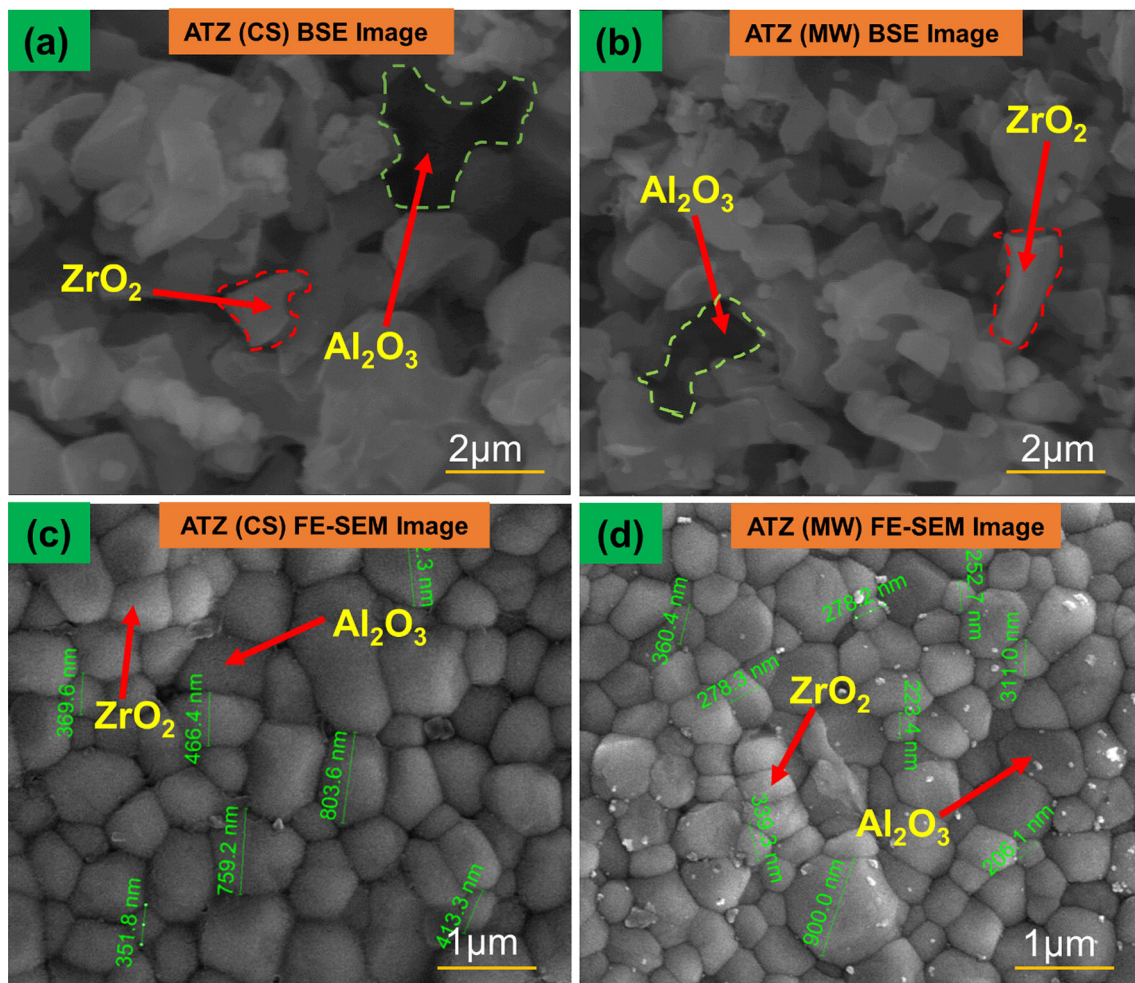


Fig. 4 The thermally etched FE-SEM microstructures of the developed ATZ composites at 1600 °C, BSE mode **a** CS and **b** MW and Normal mode **c** CS and **d** MW

densities, average grain size, microhardness, and fracture toughness as given in Table 4.

3.4 Average Grain Size

The average grain sizes of the composite samples developed through CS and MW, is given in Table 4. In the MW process, very rapid Joule heating took place in the particles compared to that of CS under pressure less condition. Therefore, the composites processed through MW showed dense microstructures and grain growth suppression compared to CS-sintered samples as shown in Fig. 4. Due to the rapid heating and high heating rate provided by MW, it did not give enough time for the grain growth leading to smaller average grain sizes in the MW samples. On the other hand, in CS composite samples, rapid heating could not be achieved due to the mode of heating employed, leading to a prolonged sintering time. Therefore, during CS, the grains had enough time to grow, resulting in a

larger average grain size. The smallest average grain size was found in the composite sample sintered through MW as shown in Fig. 4.

3.5 Relative Density

The relative densities of the developed composites are given in Table 4. As discussed earlier, very rapid and local heating with simultaneous application of load in MW led to high-density composites compared to the samples sintered using CS. However, it was observed that the relative density of the composites was well above 98.5%. The improvement in the relative density of MW composites could attributed to the very rapid heating, local particle–particle interface heating, good diffusion between the neighboring particles, quick processing time, etc.

Fig. 5 EDS spectra of ZrO₂ matrix composites reinforced with Al₂O₃ and sintered through **a** CS and **b** MW

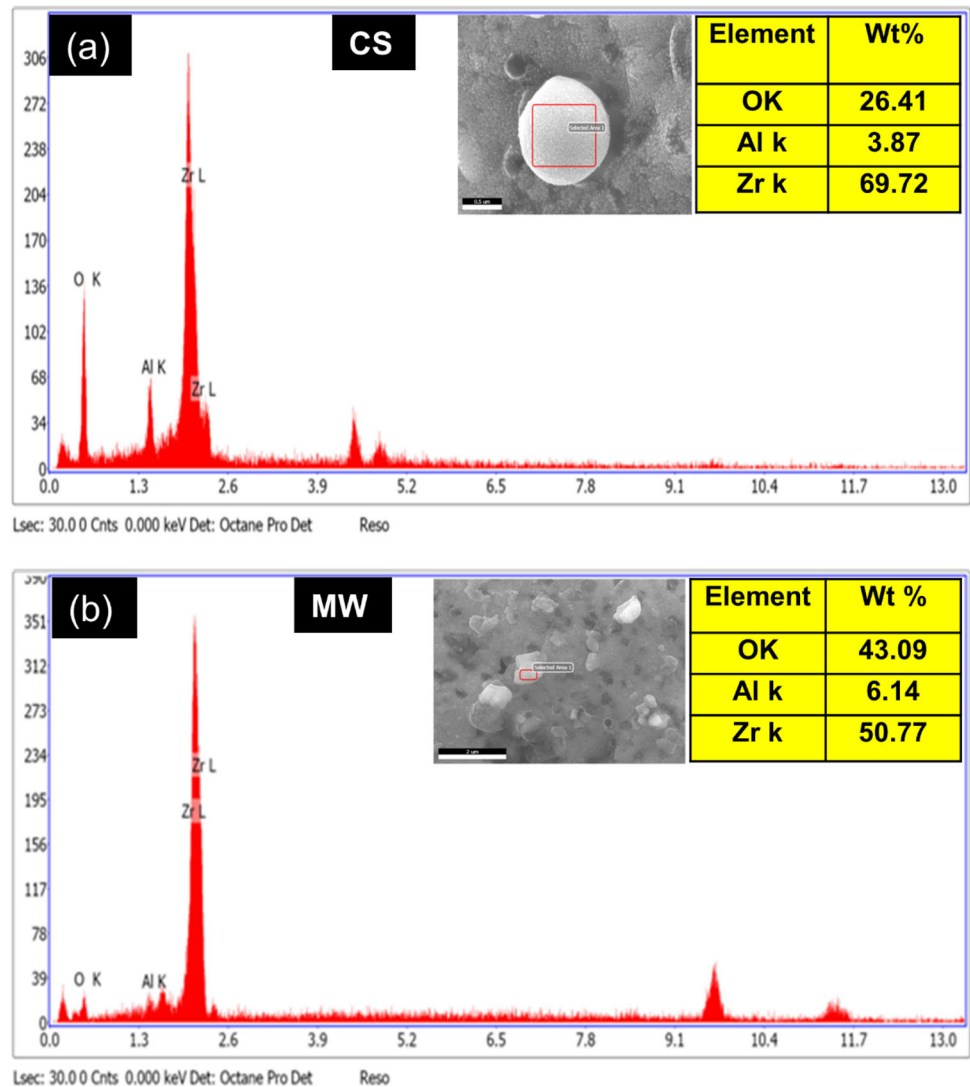


Table 4 The properties of developed ATZ composites like average grain size, relative densities, microhardness and fracture toughness

S. no.	Processes	Average grain size (μm)	Relative density (%)	Microhardness (GPa)	Fracture toughness ($\text{MPa m}^{1/2}$)
1	CS	0.511 ± 0.06	98.69 ± 0.13	17.31 ± 0.18	13.5 ± 0.99
2	MW	0.391 ± 0.04	99.11 ± 0.11	18.71 ± 0.15	14.7 ± 1.1

3.6 Microhardness

Variation in microhardness of the developed composites through MW and CS is given in Table 4. From Table 4, it could be observed that there was a trend of continuous decrease in the hardness of the composites. Composite samples sintered through MW showed higher values of microhardness. However, the presence of ZrO₂ decreased hardness, while Al₂O₃-reinforced composites exhibited increased hardness, which could be attributed to the better transformation toughening provided by ZrO₂ particles to

inhibit the grain growth of Al₂O₃ and ATZ, leading to grain suppression. Improved density and suppression of grain growth could be the reason for the improvement of hardness in the MW composite samples. The microhardness of ATZ through CS was of lower value compared to ATZ through MW.

3.7 Fracture Toughness

Variation in the fracture toughness of the composite samples developed through MW and CS is given in Table 4.

Fracture toughness is the ability of a material to resist fracture by absorbing energy and providing resistance to crack propagation. During MW, the rapid heating rate was applied, while in CS sintering, slow heating was applied in a pressure-less condition. More suppression of grain growth and dense microstructures were observed in the sintered samples through MW compared to that of the CS-sintered samples, as shown in Fig. 4. The presence of transformation toughening of ZrO₂ had reduced the monoclinic phase and increased the tetragonal phases and hence resulted in improved fracture toughness of the sintered samples [32] as shown in Fig. 3. The fracture toughness of ATZ composites developed through CS was found to be of lower value compared to MW.

3.8 Characterization of Tribological Properties

Wear test was carried out on the ATZ composite samples developed through CS and MW to evaluate the wear rate and COF by varying normal load in the range of 35–95 N and various sliding velocities (0.79 m/s, 1.4 m/s, 1.8 m/s and 2.4 m/s) for a sliding distance of 1500 m.

(a) Variation in the COF with varying normal load and sliding velocity

Variation in the COF of the developed composites with variation in the normal load in the range of 35–65 N with 0.79 m/s, 1.4 m/s, 1.8 m/s sliding velocities is shown in Fig. 6.

The COF decreased with an increase in the normal load irrespective of the sliding velocity. However, with an increase in the sliding velocity, the COF further decreased, as seen in Fig. 6. The reduction in the COF values could be attributed to the formation of a compacted tribo-layer between the pin and disk. Specifically, when the normal load increased, the oxide layer was transformed from the counter surface (disk of emery paper) to the pin (developed composite samples). It resulted in reduced COF values

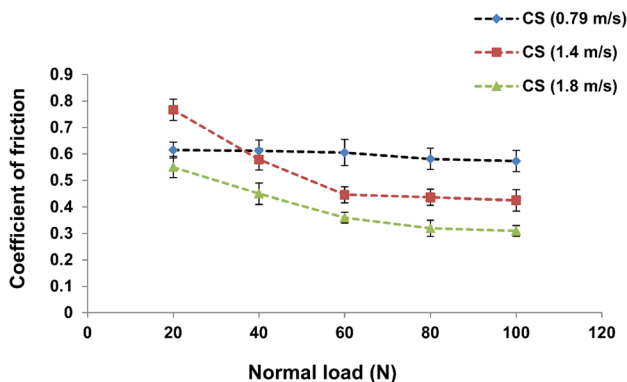


Fig. 6 Variation in COF of the CS samples with varying normal load at a sliding velocity of 0.79 m/s, 1.4 m/s, and 1.8 m/s

[33]. As compared to CS-sintered composite samples, lower values of COF were observed in the composite samples sintered through MW. The ATZ through MW composite samples showed lower values of COF compared to the ATZ through CS composites samples, as shown in Fig. 6.

(b) Variation in the wear rate with varying normal load and sliding velocity

The variation in wear rate of the developed composites with varying normal load in the range of 35–65 N at 0.79 m/s, 1.4 m/s, 1.8 m/s sliding velocities is shown in Fig. 7.

The wear rate of the developed composite samples increased with an increase in the normal load with sliding velocities of 0.79 m/s, 1.4 m/s, 1.8 m/s. The wear rate decreased with an increase in the sliding velocity and increased with an increase in the normal applied load. No tribo-layer formation was observed at low normal loading conditions, which might be the possible reason for an increase in the wear rate. However, the wear rate rapidly increased beyond 60 N for all sliding velocities. It was observed that the tribo-layer formation occurred when the applied normal load exceeded 60 N. As discussed earlier, the formation of a tribo-layer on the developed composite sample pin resulted in the reduction of wear rate. The tribo-layer of the material was transferred from the counter surface (steel disk) to the pin as a product of the environmental reaction (oxides). This tribo-layer reduced with the direct contact of pin (sintered samples) to the counter disk surface. Lower values of wear rate were observed in the composite samples sintered through MW compared to the CS composite samples, as observed from Fig. 7.

(c) Variation in COF with varying normal load and constant higher sliding velocity

The variation in the COF of the developed composite samples with varying normal load in the range of

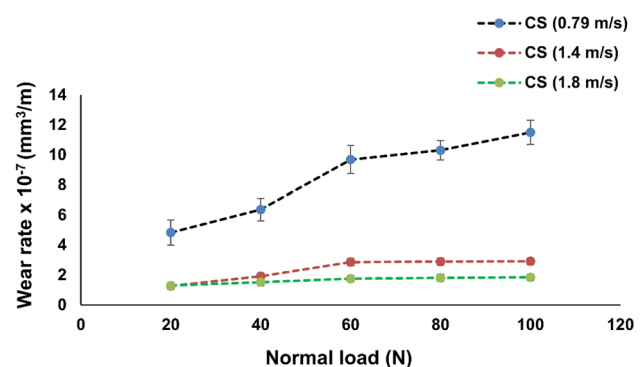


Fig. 7 Variation in the wear rate of the CS samples with varying normal load at a sliding velocity of 0.79 m/s, 1.4 m/s, and 1.8 m/s

20–200 N at a constant sliding velocity of 2.4 m/s is shown in Fig. 8.

At higher loads and higher sliding velocities, the contact pressure on the asperity tip at the contact surface increased and gave rise to flash temperatures, which allowed the wear transition and orient deformation of the asperity tips at elevated temperatures. The contact of the tribological surface was found in severe wear conditions when the possible crack propagated rapidly and subsequently activated wear particles. Thus the value of COF increased at higher loads and higher sliding velocity. The COF increased with an increase in the normal load at the sliding velocity. The COF rapidly increased at a higher sliding velocities of 2.4 m/s, which was due to the rapid removal of the rough surface at a higher sliding velocity, which led to severe plastic deformation and formation of compact trio-layer layer between the pin and disk [34]. The MW-sintered composite samples were found to show lower values of COF compared to that of the CS-sintered composite samples. The developed ATZ through MW composites exhibited lower values of COF compared to that of the composites developed through CS. The maximum values of COF were found to be 0.793 and 0.598 in the composite samples developed through CS and MW, respectively, as shown in Fig. 8. The corresponding calculation was done using Eq. (4).

$$\text{COF value of CS compared to MW} = \left[1 - \frac{(\text{COFCS}_{\text{max}})}{(\text{COFMW}_{\text{max}})} \times 100 \right] \tag{4}$$

$$\begin{aligned} \text{COF value of CS compared to MW} &= \left[1 - \frac{(0.598)}{(0.793)} \times 100 \right] \\ &= 24.59\% \end{aligned}$$

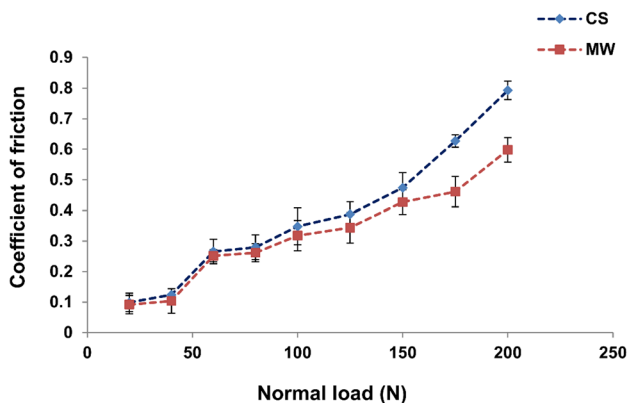


Fig. 8 Variation in the COF with varying normal load at a constant sliding velocity

where $\text{COFCS}_{\text{max}}$ = Maximum value of the coefficient of friction of CS-sintered samples, $\text{COFMW}_{\text{max}}$ = Maximum value of the coefficient of friction of MW-sintered samples.

The maximum value of the COF exhibited by the composite samples developed through MW was 24.59%, which was lower than that of the COF of conventional sintered samples.

(d) Variation in wear rate with varying normal load at a fixed higher sliding velocity

The variation in the wear rate of the developed composite samples with varying normal load in the range of 20–200 N and a constant sliding velocity of 2.4 m/s is shown in Fig. 9.

As discussed earlier, at higher load and sliding velocity, the contact pressure on the asperity tip increased giving rise to flash temperatures, which allowed wear transition and orient deformation of the asperity tips at elevated temperatures [35]. The contact of the tribological surface was found to undergo severe wear when the possible crack was propagated rapidly and subsequently activated the wear particles. Thus the wear rate increased with higher load and sliding velocities. The wear rate rapidly increased with the increase in the normal load at a sliding speed of 2.4 m/s. No tribo-layer formation was observed at low normal loading conditions, which might be the possible reason for the increase in the wear rate. However, the wear rate rapidly increased beyond the 60 N irrespective of the sliding velocity. It was observed that the tribo-layer on the surface was formed beyond 60 N. Wear transition phase occurred on cracks with plastic deformation and severe wear took place and resulted in increasing COF and wear rate. The tribo-layer consisted of material transferred from the counter surface (steel disk) to pin along with the environmental reaction products (oxides). This tribo-layer reduced the direct contact of pin (developed ATZ composite) to the counter of the disk surface.

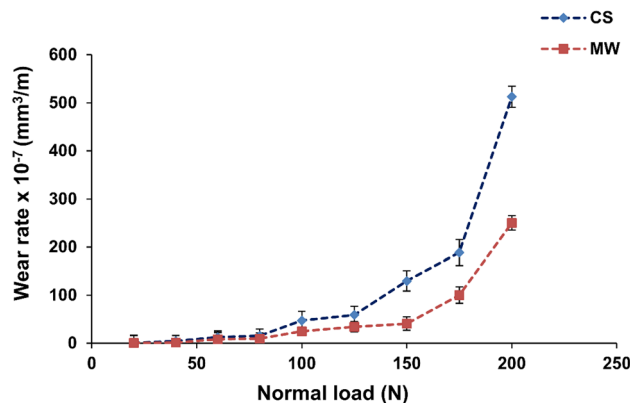


Fig. 9 Variation in the wear rate with varying normal load at a constant sliding velocity

The MW-sintered composite could have promoted a highly adhered layer at the contact surface compared to CS samples resulting in better wear resistance. The sample developed through CS had a loose layer at the contact surface, which got worn out in a shorter period leading to an increase in the wear rate. Compared to CS samples, composite samples developed through MW were found to exhibit a lower wear rate. The maximum values of the wear rate were found to be $513.09 \times 10^{-7} \text{ mm}^3/\text{m}$ and $250.33 \times 10^{-7} \text{ mm}^3/\text{m}$ in the composite samples developed through CS and MW, respectively, as shown in Fig. 9 and its corresponding calculations were done using Eq. (5).

WR value of CS compared to MW

$$= 1 - \frac{(\text{WRCS}_{\text{max}})}{(\text{WRMW}_{\text{max}})} \times 100 \quad (5)$$

$$\text{WR value of CS compared to MW} = 1 - \frac{(250.33)}{(513.09)} \times 100 \quad (6)$$

WR value of CS compared to MW = 51.21%.

where WRCS_{max} = Maximum value of wear rate of CS-sintered sample, WRMW_{max} = Maximum value of wear rate of MW-sintered sample.

The maximum value of the wear rate of 51.21% of microwave sintered samples exhibited lower values than the conventional sintered samples.

(e) Morphology of worn-out surfaces of the composite samples and AFM analysis of the composites

The FE-SEM microstructures of typical worn-out surfaces of 10 vol% alumina reinforced to the zirconia matrix are shown in Fig. 10a–d. The microstructures reveal the morphology of the wear track of CS- and MW-sintered samples at a normal load of 100 N and 200 N, respectively.

As discussed earlier, in the MW process, rapid joules heating was applied, while in CS, slow heating was applied under pressure-less conditions. Therefore, more uniform grains were observed in the samples sintered through MW when compared to the CS samples. Due to the decrease in the grain size, the hardness of the composites increased in the case of MW composite samples. The Al_2O_3 reinforcement provided an improvement in the hardness, while the ZrO_2 matrix also produced an improvement in the fracture toughness of the composite. The presence of ZrO_2 also provided suppression of grain growth by transformation toughening, leading to an increase in the hardness. Therefore, an increase in the hardness of the sample led to a hard surface providing more resistance to wear. When the applied normal load was 100 N, the worn-out surfaces of the composite samples exhibited plastic deformation

mechanism and mixed abrasion. The morphology of the worn-out surfaces of the composite samples changed from fine scratches to grooves and damaged spots. The presence of abrasion on the worn-out surfaces of the samples was found with scoring grooves along the direction of sliding. These grooves were formed due to the action of the wear-hardened particles deposited on the surface of the disk track. Further, increasing the normal load up to 200 N, it was found that the locally damaged spots and fractured spots on the surfaces were due to the inability of the protective layers of reinforcing particles to remain for a longer time.

Moreover, under the action of plowing, the composite samples were found to fracture due to severe deformation. With an increase in the normal load, the COF decreased and the wear rate increased at a sliding velocity of 2.4 m/s, which was due to the low contact between ceramic and metal. Shallow grooves were formed under a lower normal load as the loose particles entrapped between the composite sample and disk created a plowing effect. The entrapped particle in the matrix in which the loose particles were pulled out from the matrix during sliding is shown in Fig. 10a, c. The crack propagation could be observed from Fig. 10b, d. The overall depth of the plastic deformation and applied load-related linearity depended on the relation between normal load and wear rate.

In the conventional sintered composite sample, it was observed that the loose tribo-layer was formed on the surface of the sintered sample at the normal load 100 N as shown in Fig. 10a. Furthermore, at a higher normal load of 200 N, there were more uncovered tribo-batches at the tribo-surface as seen in Fig. 10b. This led to the marginally higher COF at normal loads. In the microwave sintered sample, it could be found that fewer loose tribo-layers were formed at the tribo-surface at a normal load of 100 N as shown in Fig. 10c. Furthermore, with an increase in the normal load up to 200 N, large peeled off tribo-layers could be observed, as shown in Fig. 10d, which led to more virgin composite pin to metal contact. Also, a covered adherent tribo-layer at the tribo-surface could be observed from Fig. 10d. This adherent layer reduced the frictional force between the sliding surfaces leading to a decrease in the COF. On the other hand, with an increase in the normal load, the tribo-layer that was formed was peeled off during sliding resulting in an increase in the COF. The FE-SEM microstructures of the worn surfaces of the composite samples developed through CS exhibited broad and deep grooves, several plastic deformations, and large pits, when compared to that of the composite samples, developed through MW.

Further, the wear mechanisms involved in the morphology of the worn surfaces after wear testing were demonstrated through atomic force microscopy and FE-

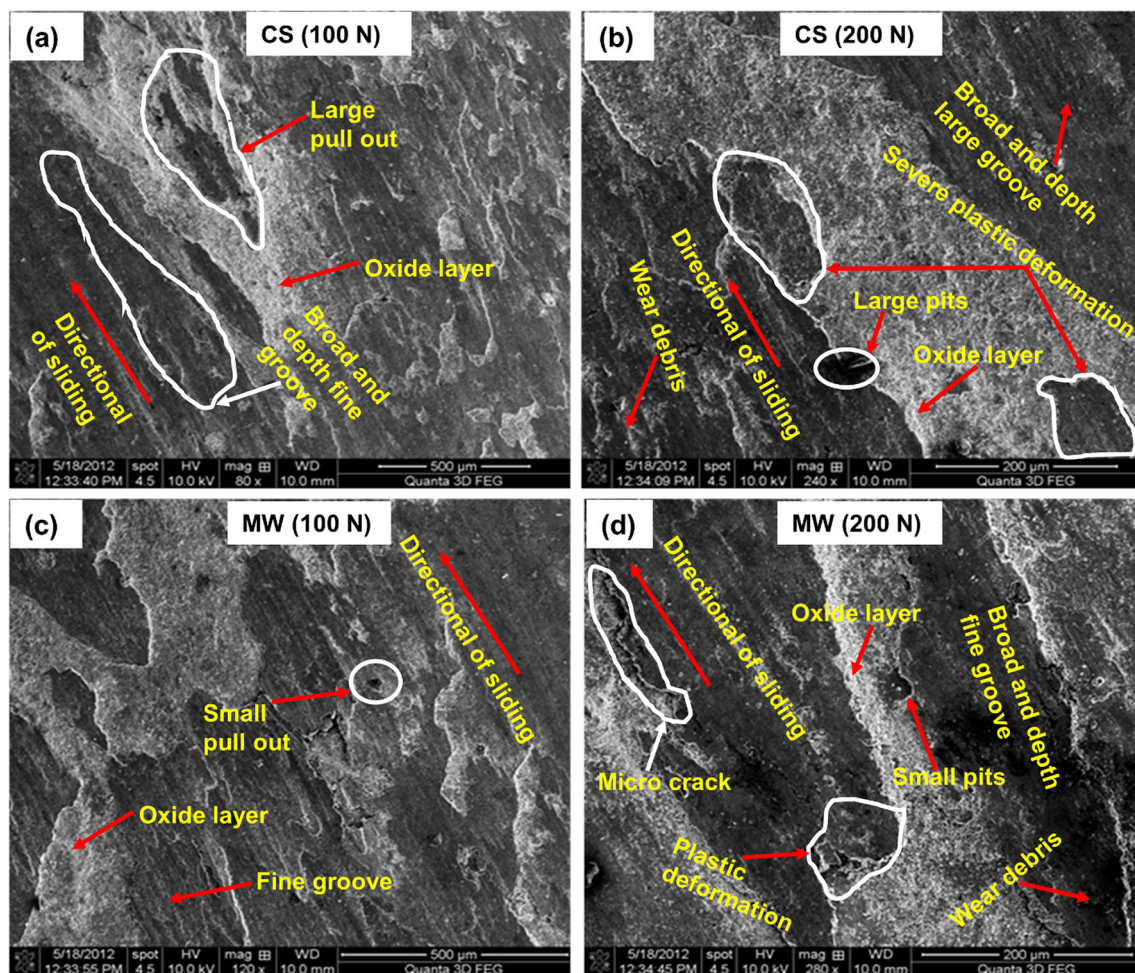


Fig. 10 FE-SEM microstructure of worn-out surfaces of the developed ATZ composite samples with a normal load of 100 N and 200 N at constant sliding velocity of 2.4 m/s **a** CS 100 N, **b** CS 200 N, **c** MW 100 N and **d** MW 200 N

SEM analysis throughout the worn-out surfaces of developed composites. AFM studies were carried out to analyze the wear topography of ATZ composite developed through CS, as shown in Fig. 11a, b and ATZ composite developed through MW, as shown in Fig. 11c, d performed at similar wear conditions. The topographical aspects of the wear surface are presented in Figs. 11 and 12, respectively. Figure 11 represented the AFM results of the worn surface of ATZ composite developed through CS at an applied normal load of 200 N for a sliding distance of 1500 m. As discussed earlier, this developed composite was observed to show maximum wear on the surfaces among the two other developed composites [36].

Since the hardness of the ATZ composite developed through the MW process was high as compared to ATZ composite developed through the CS process, the worn surface topography of the composite surfaces was entirely different. For the same applied load and sliding distance, the wearing phenomena of the ATZ composite developed through CS became more severe as compared to ATZ

composite developed through MW and the average surface roughness (R_a) of the worn surface was $0.519 \mu\text{m}$ and maximum roughness height h_{max} was $1.0 \mu\text{m}$ as shown in Fig. 11b. The severe wear of the composite sample could be attributed to the decrease in the hardness value and an increase in the actual area of contact between the abrasive and sample surface. Consequently, the flow stress reduced [36] concerning abrasive and wear surface, which promoted maximum indentation of abrasive particles on the ceramic matrix, followed by an increase in coefficient of friction and groove width, as seen from Fig. 11c. Figure 12 shows the worn surface for the ATZ and their respective AFM topography of the composite developed through MW with an applied normal load 100 N for a sliding distance of 1500 m, as discussed earlier. As discussed earlier, this developed composite was observed to show minimum wear on the surfaces among the two other developed composites.

The wear scars developed on the composite 2D surface are as shown in Fig. 12a. The maximum surface roughness peaks ($h_{\text{max}} = 0.22 \mu\text{m}$), as shown in Fig. 12c, were due to

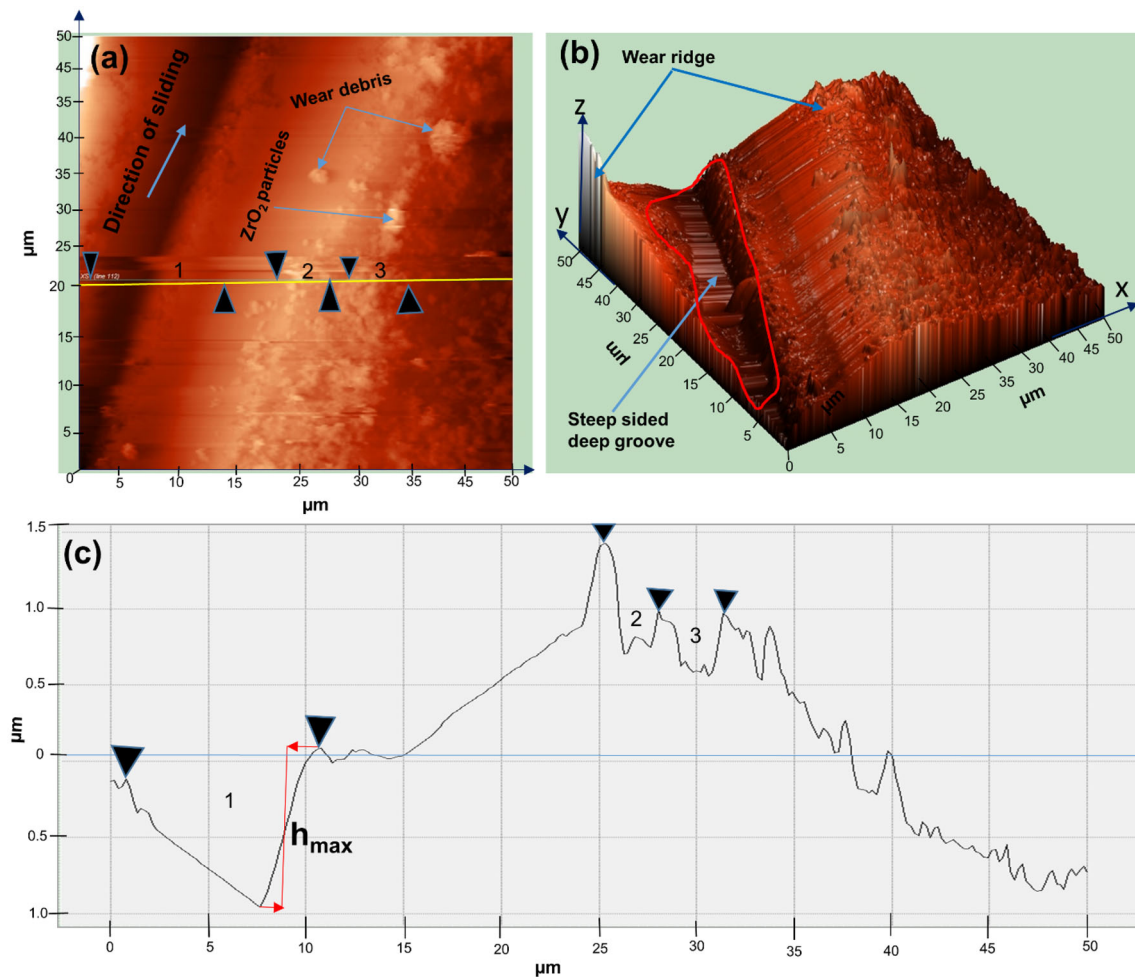


Fig. 11 AFM results indicating the worn surface profile with x-axis direction of ATZ through CS at an applied load of 200 N and sliding distance 1500 m: **a** 2D surface topography, **b** corresponding isometric 3D surface topography, **c** line surface profile indicating the position of the line on **a**

the steep side deep groove formation, which might have occurred due to the axial overload during sliding. Concerning the above abrasive wear parameters, experimental results revealed that the volumetric wear rate was low and on the other hand, the coefficient of friction was high. From the topography, it was evident that the groove widths were relatively constant and average surface roughness of about 0.209 μm were found.

4 Conclusions

Based on the present investigation, the following major conclusions could be drawn:

- Full density was achieved in the composite samples sintered through MW as compared to CS composite samples, which also yielded decent relative density.
- XRD analysis revealed that the presence of transformation toughening of ZrO₂ reduced the monoclinic phase and increased the tetragonal phases and hence resulted in improved fracture toughness of the developed composite samples. However, full density and suppression of grain growth along with the pinning effect improved the fracture toughness of the MW samples when compared to that of the CS composite samples.
- The tribological properties of the composite samples developed through MW were enhanced remarkably when compared to that of the composite samples developed through CS. The MW-sintered composite could have promoted a highly adhered layer at the contact surface compared to CS-sintered samples resulting in better wear resistance. On the other hand, at lower normal load conditions, no tribo-layer formation was observed, which could be the possible reason for the increase in the wear rate.

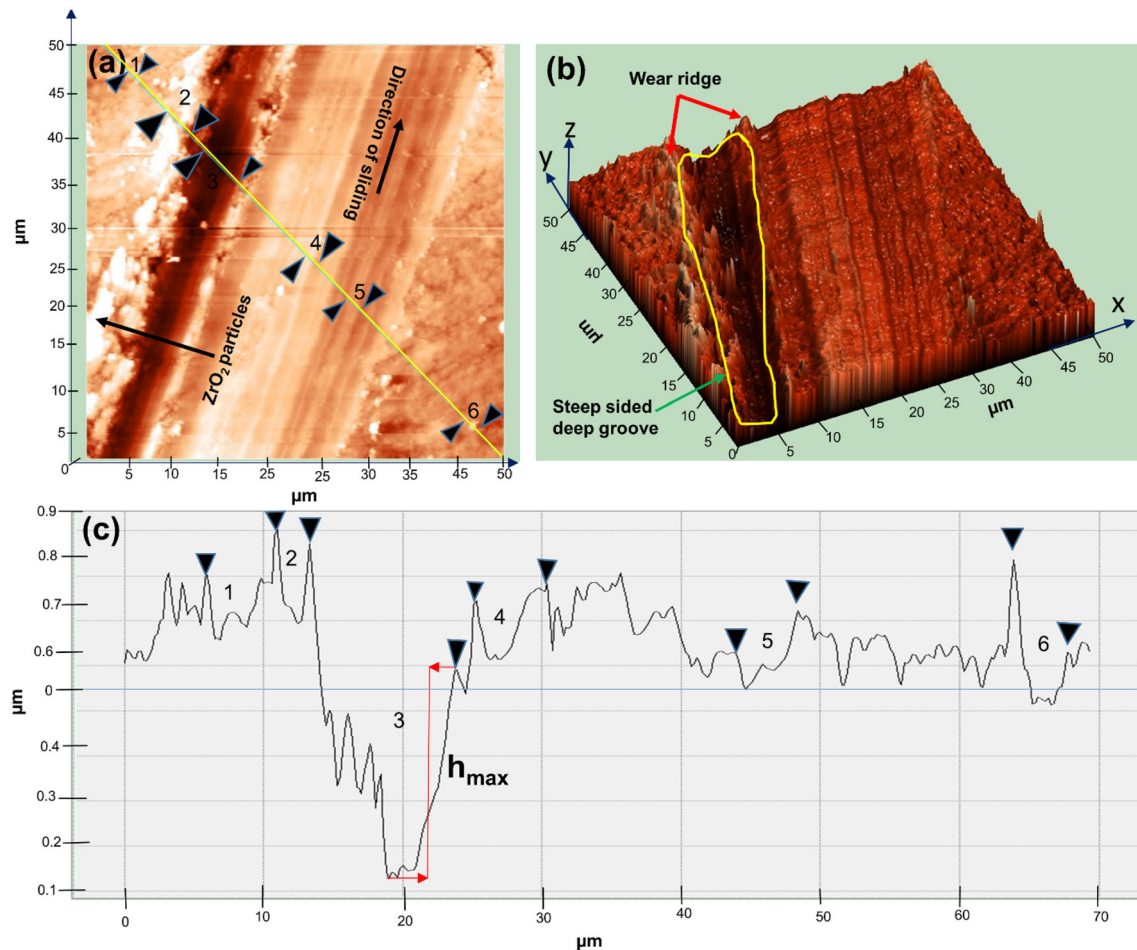


Fig. 12 The AFM results indicating the worn surface profile with the inclined direction of ATZ through MW at an applied load of 100 N and sliding distance 1500 m: **a** 2D surface topography, **b** corresponding isometric 3D surface topography, **c** a line surface profile indicating the position of the line on **a**

- With lower values of wear parameters, the COF decreased and the wear rate increased with an increase in the normal loads and sliding velocity. On the other hand, with higher values of wear parameters, the wear rate and COF increased with an increase in the normal loads and sliding velocity due to the rapid removal of the rough surface at a higher sliding velocity, which led to severe plastic deformation and formation of compact trio-layer layer between the pin and disk. However, the wear rate rapidly increased beyond a normal load of 60 N irrespective of the sliding velocity.
- During the wear test of CS composite samples, the top layers of the samples (pin) wore out at the contact surface in a shorter period as they were loosely bonded, and hence, the COF values of the CS samples were found to be higher than that of the MW composite samples.
- The values of the COF and wear rate of developed ATZ composites through MW were lower than that of the composites developed through CS.
- The maximum value of the wear rate and the COF of the MW composite sample was calculated to be 51.21% and 24.59%, respectively, which were lower compared to the CS composite samples.

Acknowledgements The authors would like to thank the Ministry of Human Resources and Development (MHRD), Government of India and Indian Institute of Technology Roorkee, India.

References

1. Cahoon H P, and Christensen C J, *J Am Ceram Soc* **39** (1956) 337. <https://doi.org/10.1111/j.1151-2916.1956.tb15599.x>.
2. Claussen N, and Steeb J, *J Am Ceram Soc* **59** (1976) 457. <https://doi.org/10.1111/j.1151-2916.1976.Tb09524.x>.
3. Stevens R, *J Mater Sci* **24** (1989) 3421.

4. Zhang W, Chen H, and Prentki R, *Comput Mater Sci* **137** (2017) 153. <https://doi.org/10.1016/j.commatsci.2017.05.021>.
5. Jeevan V, Rao C S P, Selvaraj N, and Rao G B, *Mater Today Proc* **5** (2018) 254. <https://doi.org/10.1016/j.matpr.2017.11.080>.
6. Du J, Chong X, Jiang Y, and Feng J, *Int J Heat Mass Transf* **89** (2015) 872. <https://doi.org/10.1016/j.ijheatmasstransfer.2015.05.046>.
7. Gutierrez-Gonzalez C F, and Bartolome J F, *J Mater Res* **23** (2008) 570. <https://doi.org/10.1557/jmr.2008.0075>.
8. Qiu B, Xing S, and Dong Q, *Metals* **9** (2019) 986. <https://doi.org/10.3390/met9090986>.
9. Perrichon A, Liu B H, Gremillard L, Reynard B, Liao J, and Geringer J, *Materials* **10** (2017) 569. <https://doi.org/10.3390/ma10060569>.
10. Zhang F, Vanmeensel K, Inokoshi M, Batuk M, Hadermann J, Van Meerbeek B, and Vleugels J, *J Eur Ceram Soc* **35** (2015) 741. <https://doi.org/10.1016/j.jeurceramsoc.2014.09.018>.
11. Rittidech A, Somrit R, and Tunkasiri T, *Ceram Int* **39** (2013) S433. <https://doi.org/10.1016/j.ceramint.2012.10.108>.
12. Basha A S, Chandra K S, and Sarkar D, *J Alloys Comput* **829** (2020) 1545592. <https://doi.org/10.1016/j.jallcom.2020.154559>.
13. Bansal N P, NASA/TM (2003) 212451.
14. Kato K, and Adachi K, *Wear* **253** (2002) 1097.
15. Kato K, *Proc Inst Mech Eng Part J: J Eng Tribol* **216** (2002) 349.
16. Hamilton G M, *J Appl Mech* **6** (1966) 371.
17. Huang S, Binner J, Vaidhyanathan B, Brown P, Hampson C, and Spacie C, *Adv ceram Arm* **32** (2011) 103. <https://doi.org/10.1002/9781118095256.ch10>.
18. Ratnam M M, and Ahmad Z A, *Adv Mater Res* 1662–8985 (2014) 101. <https://doi.org/10.4028/www.scientific.net/AMR.1087.101>.
19. Palmero P, Montanaro L, Reveron H, and Chevalier J, *Materials* **7** (2014) 5012. <https://doi.org/10.3390/ma7075012>.
20. Al Mahmood A, Gafur MA, and Hoque ME, *Mater Sci Eng A* **707** (2017) 118. <https://doi.org/10.1016/j.msea.2017.09.048>.
21. Ahmad, A Z, Mohamad H, Ratnam M, and Ahmad Z, *J Alloy Compd* **497** (2010) 316. <https://doi.org/10.1016/j.jallcom.2010.03.054>.
22. Meena K L, and Karunakar D B, *Int J Refract Met Hard Mater* **81** (2019) 281. <https://doi.org/10.1016/j.jrmhm.2019.03.009>.
23. Azhar A Z A, Mohamad H, Ratnam M M, and Ahmad Z A, *J Alloys Compd* **497** (2010) 316. <https://doi.org/10.1016/j.jallcom.2010.03.054>.
24. De Couto C A O, Ribeiro S, and Passador F R, *Ceramica* **64** (2018) 608. <https://doi.org/10.1590/0366-69132018643722475>.
25. Kitchen H J, Vallance S R, Kennedy J L, Tapia-Ruiz N, Carassiti L, Harrison A, and Gregory D H, *Chem Rev* **114** (2014) 1170. <https://doi.org/10.1021/cr4002353>.
26. Oghbaei M, and Mirzaee O, *J Alloy Compd* **494** (2010) 175. <https://doi.org/10.1016/j.jallcom.2010.01.068>.
27. Cheng J, Agrawal D, Zhang Y, and Roy R, *Mater Lett* **56** (2002) 587. [https://doi.org/10.1016/S0167-577X\(02\)00557-8](https://doi.org/10.1016/S0167-577X(02)00557-8).
28. Taffner U, Carle V, and Schafer U, *ASM Int* **9** (2004) 1057. <https://doi.org/10.1361/asmhba000379>.
29. Sarkar D, *Compos Part A: Appl Sci Manuf* **38** (2007) 124. <https://doi.org/10.1016/j.compositesa.2006.01.005>.
30. Chowdhury M A, Nuruzzaman D M, Mia A H, and Rahaman M L, *Tribol Ind* **34** (2012) 18.
31. Kumar M, Megalingam M A, Baskaran V, and Ramji K S H, *J Eng Tribol* **230** (2015) 402.
32. Michalek M, Sedlacek J, Parchoviansky M, Michalkova M, and Galusek D, *Ceram Int* **40** (2014) 1289. <https://doi.org/10.1016/j.ceramint.2013.07.008>.
33. Ravikiran A, Subbanna G, and Bai BP, *Wear* **192** (1996) 56.
34. Wang Y, He C, Hockey B, Lacey P, and Hsu S, *Wear* **181** (1995) 156.
35. Senda T, Drennan J, McPherson R, *J Am Ceram Soc* **78** (1995) 3018.
36. Sujith S V, Mahapatra M M, and Mulik R S, *Proc Inst Mech E Part J: J Eng Tribol* **0** (2019) 1.

Publisher's Note Springer Nature remains neutral with regard to jurisdictional claims in published maps and institutional affiliations.